JOC The Journal of Organic Chemistry

Article

Mechanistic Insights into the Chemo- and Regio-selective B(C6F5)3 Catalyzed C-H Functionalization of Phenols with Diazoesters

Qi Zhang, Xiaofei Zhang, Mo Li, Cheng Li, Jia-Qin Liu, Yuan-Ye Jiang, Xin Ji, Lu Liu, and Yu-Cheng Wu

J. Org. Chem., **Just Accepted Manuscript** • Publication Date (Web): 22 Oct 2019

is published by the American Chemical Society. 1155 Sixteenth Street N.W., Washington, DC 20036

Mechanistic Insights into the Chemo- and Regio-selective $B(C_6F_5)_3$ Catalyzed C−H Functionalization of Phenols with Diazoesters

Qi Zhang, [a‡] Xiao-Fei Zhang, [a‡] Mo Li, [a] Cheng Li,[a] Jia-Qin Liu,*[a] Yuan-Ye Jiang,*[b] Xin Ji,[c] Lu Liu,[c] Yu-Cheng Wu [d]

[a] *Anhui Province Key Lab of Aerospace Structural Parts Forming Technology and Equipment, Institute of Industry & Equipment Technology, Hefei University of Technology, Hefei 230009, China*

[b] *School of Chemistry and Chemical Engineering, Qufu Normal University, Qufu 273165, China*

[c] *School of Chemistry and Molecular Engineering, East China Normal University, Shanghai, 200241, China*

[d] *School of Materials Science and Engineering, Hefei University of Technology, Hefei 230009, China*

Emails: jqliu@hfut.edu.cn; qfnu_yuanyejiang@163.com

Table of Contents

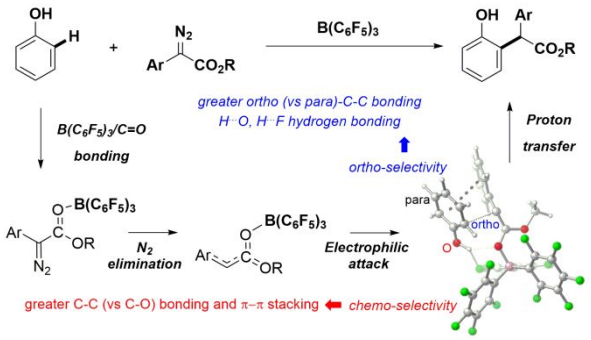

Abstract

The Lewis acidic $B(C_6F_5)_3$ was recently demonstrated to be effective for the C−H alkylation of phenols with diazoesters. The method avoids the general hydroxyl activation in transition metal catalysis. O*rtho*-selective C−H alkylation occurs regardless of potential *para*-selective C−H alkylation and O−H alkylation. In the present study, a theoretical calculation was carried out to elucidate the reaction mechanism and the origin of chemo- and regio-selectivity. It is found that the previously-proposed $B(C_6F_5)_3$/N or $B(C_6F_5)_3$/C bonding-involved mechanisms are not favorable, and a more favored one involves the $B(C_6F_5)_3$/C=O bonding, rate-determining N_2 elimination, selectivity-determining electrophilic attack and proton transfer steps. Meanwhile, the new mechanism is consistent with KIE and competition experiments. The facility of the mechanism is attributed from two factors: First, the $B(C_6F_5)_3$/C=O bonding reduces the steric hindrance during electrophilic attack. Second, the bonding forms the conjugated system by which the LUMO energy is reduced via the electron-withdrawing $B(C_6F_5)_3$. The *ortho*-selectivity is resulted from the greater *ortho*-C-C (than *para*-C-C) interaction and the O−H···O and O−H···F hydrogen bond interaction during electrophilic attack. The greater C-C (than C-O) interaction and the π-π stacking between the benzene rings of phenol and diazoester concerted contribute to the chemo-selective C−H alkylation.

1. Introduction

C−H activation/functionalization reaction is a versatile and atom economic tool to convert relatively inert C−H bonds into C−C and C−heteroatom bonds[1-3]. The method has been widely applied in the synthesis of high value-added chemicals such as drugs, natural products and polymer materials.[4-5] Despite of the countless successful examples achieved with transition metal catalysts,[6,7] increasing attention has been paid to C−H activation/functionalization with more sustainable and environment-friendly systems. In this context, C−H functionalization catalyzed by metal-free boron Lewis acids (such as $B(C_6F_5)_3$ and $B(C_6F_5)_nH_m$) which are less toxic, cheaper than transition metal catalysts, has been regarded as a promising solution.[8,9] Along with the development of this field, the construction of C−C and C−heteroatom bonds was realized for a wide range of substrates like the C(sp)−H bonds of aryl-, alkyl- and silicon-substituted alkynes,[10] and the active $C(sp^3)$ −H bonds of allyl, benzyl and alkylamines.[11]

The $C(sp^2)$−H bond activation/functionalization for modification of the (hetero)aromatic rings generally spreads in the synthesis of pharmacologically active structures.[12] Interestingly, for the $C(sp^2)$−H bond activation/functionalization, recent studies reveal that metal-free boron Lewis acid catalysis not only has advantages in price and safety,[13] but also reveals different characteristics to the well-established transition-metal-catalytic reactions.[14] For instance, using diazoesters as alkylation reagents, the alkylation of intrinsically active phenolic O−H bonds was extensively reported for various metal catalysts based on Rh[15], Cu[16], Ru[17], Fe[18] and Pd[19] (Scheme 1a). On the other hand, Zhang[20] and Shi[21] disclosed the selective C−H alkylation at the less steric-hindered *para* position of phenols with Au catalysts (Scheme 1b). Different to the above cases, Zhang et al. reported the challenging *ortho*-selective C−H alkylation of phenols with $B(C_6F_5)_3$ as Lewis acid catalyst (Scheme 1c).[22] This method avoids the general activation of hydroxyl group in the transition metal catalysis, and provides an important route for the *ortho*-substitution of unprotected phenolic C−H bonds.

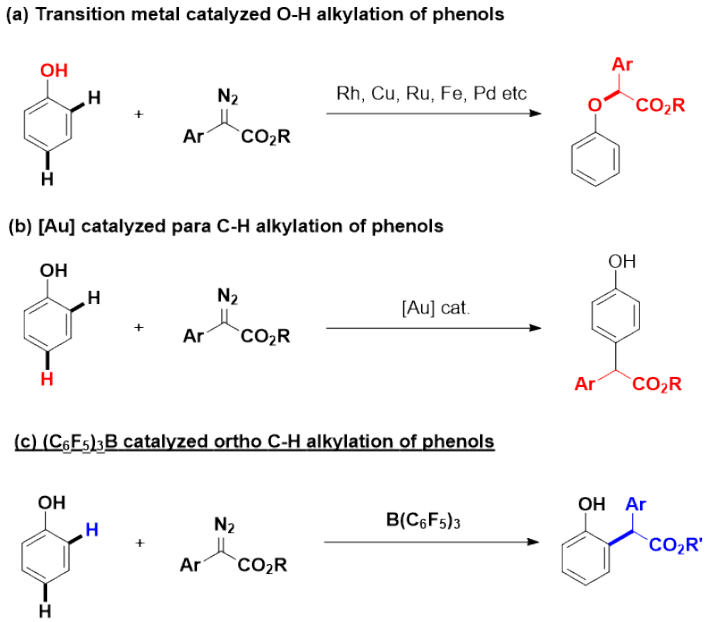

Scheme 1 Transformations of phenols with different catalysts

To explore the origin of *ortho*-selective C−H alkylation, preliminary mechanistic study with NMR spectra was conducted by Zhang group.[22] It was found that increasing the amount of phenol shifted the ^{19}F resonance to downfield, but did not change the ^{11}B resonance. In addition, the *ortho*-selectivity disappeared when the anisole substrate was used, suggesting that the F···H−O hydrogen bond between $B(C_6F_5)_3$ and phenol contributes to the *ortho*-selectivity. To further clarify the mechanism, the authors conducted kinetic isotope experiments. The k_H/k_D=0.85:1 reveals that C−H cleavage may undergo electrophilic addition and is not the rate-determining step. Further, with hydroxyl-deuterated phenol as substrate, the α-position of the acetate in the product was partially deuterated, showing that hydroxyl group acts as a proton source. Accordingly, Zhang et al. proposed that $B(C_6F_5)_3$ first bonds with the nitrogen atom of the diazoester substrate (Path A, Scheme 2). The activated carbon atom of diazoester attacks the *ortho*-carbon of phenol to form carbon-carbon bond. The C-H bond cleavage and N_2 dissociation finally occur to give alkylation product. Considering the different activation modes of diazoester, Zhang group also proposed "$B(C_6F_5)_3$/C bonding-electrophilic attack-C−H cleavage" process (Path B, Scheme 2). Different from Path A, $B(C_6F_5)_3$ first bonds with the carbon atom of diazoester. The activated carbon attacks the *ortho*-carbon of phenol. Finally, the C−H bond cleavage and N_2 dissociation occur to give product.

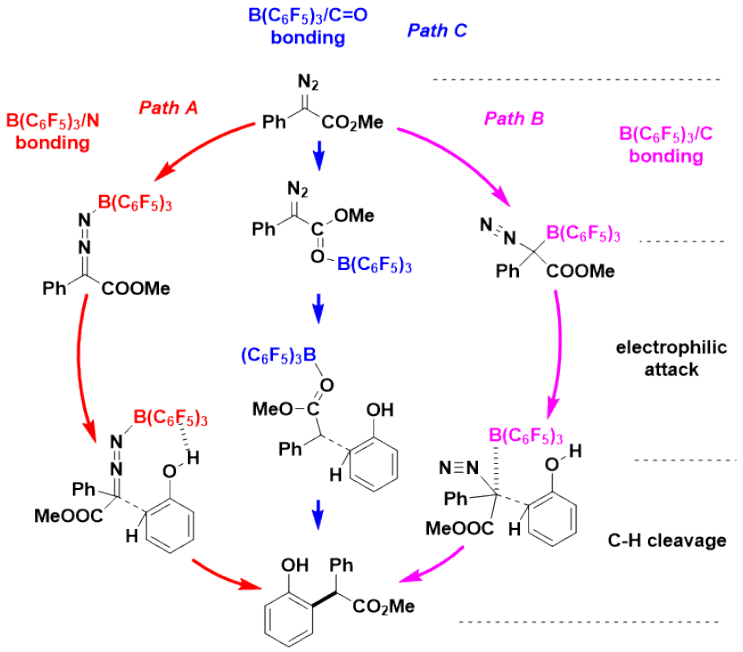

Scheme 2 The possible mechanisms of the $B(C_6F_5)_3$ catalyzed C-H functionalization of phenols

Despite the above experiments and mechanism proposals, the specific mechanism of $B(C_6F_5)_3$ catalyzed alkylation between phenol and diazoester is still unclear. On one hand, it is uncertain between Path A and Path B. The $B(C_6F_5)_3$/N or $B(C_6F_5)_3$/C bonding triggers two completely different mechanisms. On the other hand, considering the smaller steric hindrance caused by $B(C_6F_5)_3$/carbonyl bonding, the "$B(C_6F_5)_3$/C=O bonding-electrophilic attack-C−H cleavage" process should also be taken into account (Path C, Scheme 2). For the regio-selectivity of the reaction (*ortho* vs *para* C-H alkylation), the NMR spectra of the $B(C_6F_5)_3$ and phenol mixture cannot reflect the real situation of the reaction with various substrates. Thus the role of F⋯H−O hydrogen bond between $B(C_6F_5)_3$ and phenol could not be confirmed. For the chemo-selectivity (C−H vs O-H alkylation), the unclear reaction mechanism makes it impossible to explain the reason for avoiding the hydroxyl activation. In order to solve the above problems, we carried out theoretical calculations on the mechanism of $B(C_6F_5)_3$ catalyzed phenol alkylation with diazoester. The specific reaction mechanism and origin of the regio- and chemo-selectivity are aimed to be clarified. The detailed processes of Path A (Section 3.1), Path B (Section 3.2) and Path C (Section 3.3) were investigated. Section 3.4 shows the comparison of these three mechanisms. Based on the favorable mechanism, the origins for *ortho*-selectivity and chemo-selectivity were further explained (Section 3.5).

2. Computational methods and model reaction

2.1 Computational methods

The Gaussian09 suite of programmes[23] was used for the calculations in this study. The B3LYP[24-25] method combined with the 6-31G* basis set was used for unrestricted geometry optimization in dichloromethane solvent (consistent with the experiment,[22] with SMD[26] model) on all structures. To get the thermodynamic corrections of Gibbs free energy and verify the stationary points to be local minima or saddle points, we conducted frequency analysis at the same level with optimization. For all transition states, we performed the intrinsic reaction coordinate (IRC) analysis to confirm that they connect the correct reactants and products on the potential energy surfaces.[27] M06-2X[28]/6-311++G** method with the SMD[26] model was used for the solution phase single-point energy calculations of all these stationary points (dichloromethane is used as solvent). All energetics involved in this study are calculated by adding the Gibbs free energy correction calculated at B3LYP/6-31G* and the single-point energy calculated at the M06-2X/6-311++G** method.[29]

2.2 Model reaction

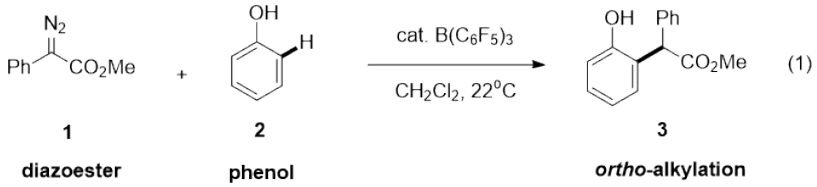

In accordance with the experimental work,[22] the reaction of diazoester **1** and phenol **2** generating *ortho*-C−H bond alkylation product **3** (eq 1) was chosen as the model reaction. $B(C_6F_5)_3$, and CH_2Cl_2 are the catalyst and solvent as used in the experiment, respectively.

3. Results and Discussions

3.1 Mechanism of Path A ($B(C_6F_5)_3$/N bonding involved)

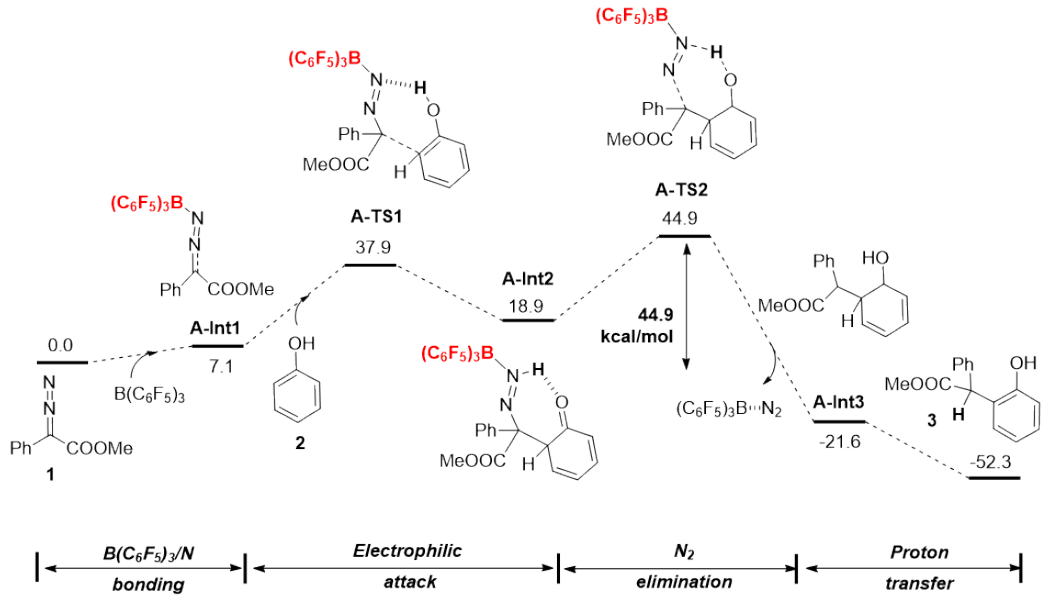

Figure 1 The energy profiles of $B(C_6F_5)_3$/N bonding involved mechanism (Path A, in kcal/mol)

As described in the introduction, for Path A, $B(C_6F_5)_3$ first bonds with the nitrogen atom of diazoester, the activated diazoester attacks the *ortho*-carbon of phenol, C-H bond cleavage and N_2 dissociation finally occur to deliver alkylation product. As shown in Figure 1, $B(C_6F_5)_3$ first coordinates with the terminal nitrogen atom of diazoester **1** to give **A-Int1** with increased free energy of 7.1 kcal/mol. After coordination, the N1−N2 bond stretches to 1.16 Å (from 1.14 Å in substrate **1**). The C1−N1−N2 angle decreases to 173.8° (from 179.1° of **1**). In addition, the Mulliken charge[30] of C1 atom changes to 0.15813 (from 0.11434 of **1**). The coordination of Lewis acidic $B(C_6F_5)_3$ to terminal N2 atom leads to slight bending of **1** and stronger eletrophilicity of C1 atom, facilitating the following electrophilic attack to phenol.

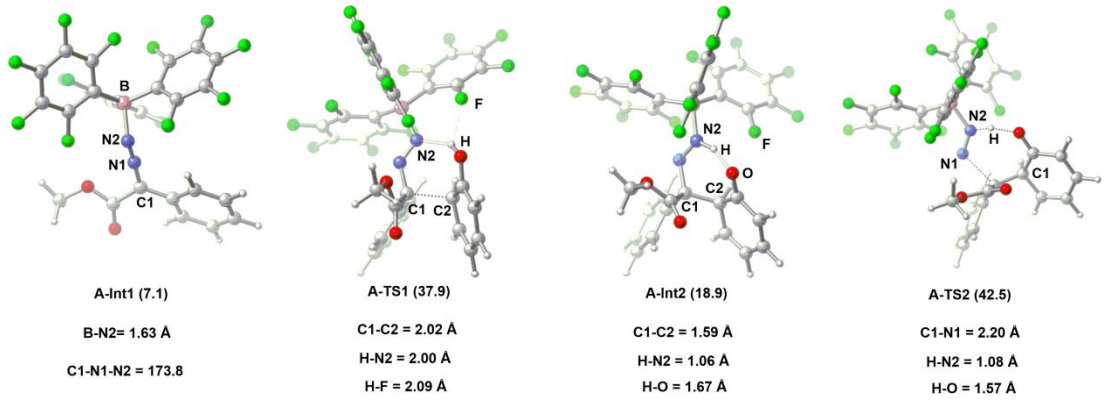

Figure 2 Optimized structures for selected species of Path A. Bond lengths are given in Å

The following electrophilic attack occurs via C1−C2 bonding transition state **A-TS1** with

free energy of 37.9 kcal/mol. The free energy barrier of the electrophilic attack step is 37.9 kcal/mol (**1→A-TS1**). In the transition state, the C1 atom of **A-Int1** attacks the *ortho*-C2 atom of phenol substrate **2**, with C1−C2 distance of 2.02 Å (Figure 2). Additionally, the O-H ⋯ N hydrogen bond exists between –OH group and terminal N2 atom with H⋯N2 distance of 2.00 Å.[31] The O-H⋯F hydrogen bond exists between -OH and -C_6F_5 group with H⋯F distance of 2.09 Å. After the electrophilic attack, **A-Int2** is formed with shortened C1−C2 bond length of 1.59 Å and free energy of 18.9 kcal/mol. Interestingly, the H atom of -OH group automatically transfers to N2 to form N2−H bond. The N-H⋯O hydrogen bond exists between N2-H and O with H⋯O distance of 1.67 Å (Figure 2). After the electrophilic attack step, the *ortho*-C−H bond is activated. Before the C-H bond cleavage, N_2 group should be eliminated to create the site for the transferred hydrogen atom. Therefore, **A-Int2** first goes through transition state **A-TS2** to dissociate $B(C_6F_5)_3$ complexed N_2. The free energy of **A-TS2** is 44.9 kcal/mol, and the energy barrier is 44.9 kcal/mol (**1→A-TS2**). In the transition state, the C1−N1 bond cleavage proceeds simultaneously with the H atom transfer from N2 to O. The C1−N1 and N2−H bond stretch to 2.20 Å and 1.08 Å, and the O−H bond shortens to 1.57 Å, respectively. After dissociation, intermediate **A-Int3** is obtained with significantly decreased free energy of -21.6 kcal/mol. The facile proton transfer from *ortho*-C atom to C1 atom then occurs on **A-Int3** to generate product **3**. The free energy further decreases to -52.3 kcal/mol.

In summary, Path A successively undergoes $B(C_6F_5)_3$/N coordination, electrophilic attack, N_2 elimination and proton transfer steps. The overall energy changes is -52.3 kcal/mol (**1→3**). The rate-determining step is N_2 dissociation with total energy barrier of 44.9 kcal/mol (**1→A-TS2**).

3.2 Mechanism of Path B ($B(C_6F_5)_3$/C bonding involved)

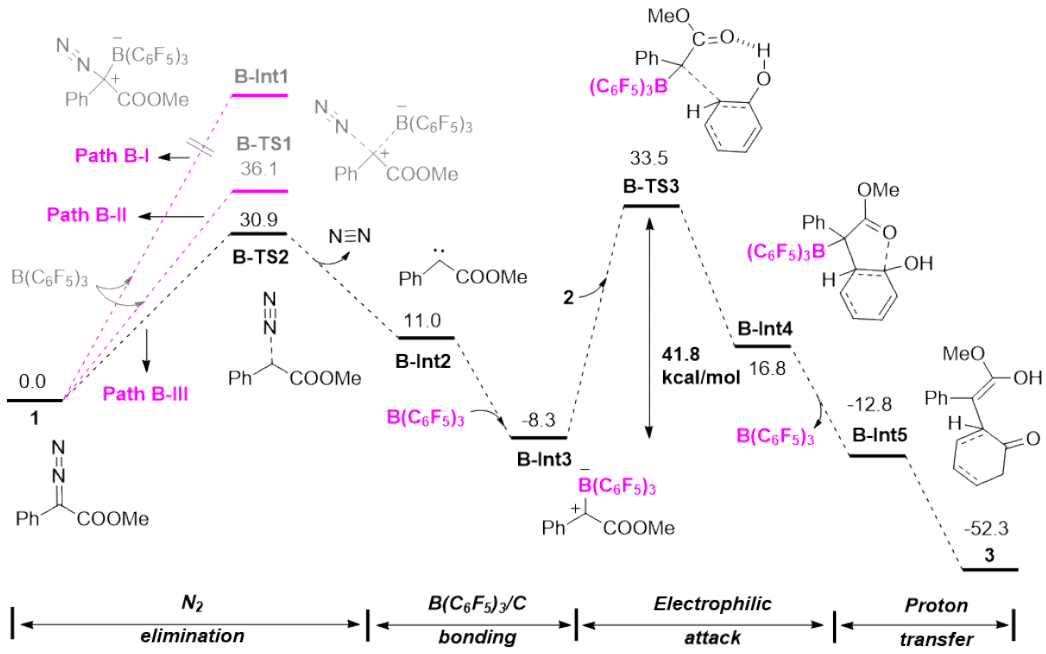

Figure 3 The energy profiles of $B(C_6F_5)_3$/C bonding involved mechanism (Path B, in kcal/mol)

As mentioned in the introduction, the "$B(C_6F_5)_3$/C bonding-electrophilic attack-C−H cleavage" process was proposed for Path B. Firstly, we investigated the mechanism that $B(C_6F_5)_3$ directly bonds with C1 atom of **1** to give B-C1 bonded intermediate **B-Int1** (Path B-I, Figure 3). However, due to the large steric hindrance between $B(C_6F_5)_3$ and diazoester, the B-C1 bond breaks automatically during optimization. To reduce the steric hindrance, we further investigated the concerted process of $B(C_6F_5)_3$ approaching and N_2 dissociation (Path B-II, Figure 3). During the optimization of the concerted transition state **B-TS1**, $B(C_6F_5)_3$ gets far away from C1, and N_2 bonds with C1 again. To estimate the energy requirement, we performed the energy scan of the B-C1 bonding process.[32] The highest energy was obtained with B-C1 bond length of 1.800 Å, and the corresponding free energy is 36.1 kcal/mol. Accordingly, both Path B-I (direct $B(C_6F_5)_3$/C1 bonding) and Path B-II (concerted bonding-N_2 dissociation) are unfavorable for the reaction.

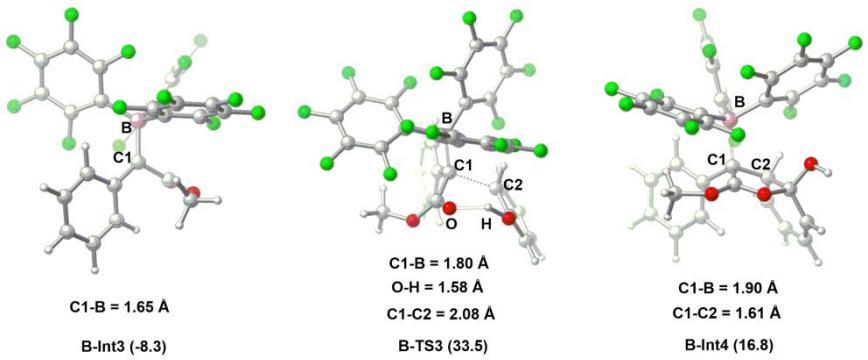

Figure 4 Optimized structures for selected species of Path B. Bond lengths are given in Å

Considering the advance N_2 dissociation would reduce the steric hindrance of $B(C_6F_5)_3$/C1 bonding, we further investigated the successive N_2 dissociation-$B(C_6F_5)_3$/C1 bonding process (Path B-III). As shown in Figure 3, from substrate **1**, the N_2 dissociation occurs first via C1−N cleavage transition state **B-TS2** with free energy of 30.9 kcal/mol. In **B-TS2**, the C1−N bond stretches to 1.60 Å from 1.32 Å of substrate **1**. After N_2 dissociation, the carbene intermediate **B-Int2** is obtained with free energy of 11.0 kcal/mol. Then, $B(C_6F_5)_3$ bonds with C1 atom of **B-Int2** to give intermediate **B-Int3** with B−C1 bond length of 1.65 Å (Figure 4). The decreased free energy of -8.3 kcal/mol for **B-Int3** indicates that the $B(C_6F_5)_3$/C bonding is exergonic.

From **B-Int3**, electrophilic attack occurs via C1−C2 bonding transition state **B-TS3**, in which C1 atom of **B-Int3** attacks the *ortho*-C2 atom of phenol. As shown in Figure 4, in the transition state, the C1-C2 bond length is 2.08 Å and the B−C1 bond stretches to 1.80 Å. The O-H⋯O hydrogen bond exists between the -OH group and carbonyl O atom with H⋯O distance of 1.58 Å. The free energy of **B-TS3** is 33.5 kcal/mol, and the corresponding energy barrier is 41.8 kcal/mol (**B-Int3** → **B-TS3**). After electrophilic attack, the intermediate **B-Int4** is obtained with formed C1−C2 bond of 1.61 Å and stretched B-C1 bond of 1.90 Å. Interestingly, in **B-Int4**, the carbonyl oxygen automatically bonds to the benzene ring to form a benzo five-membered ring with O−C distance of 1.52 Å. The free energy of **B-Int4** is 16.8 kcal/mol. Then, the facile dissociation of $B(C_6F_5)_3$ affords intermediate **B-Int5** with decreased free energy of -12.8 kcal/mol. Finally, intramolecular proton transfer occurs to give product **3** with decreased free energy of -52.3 kcal/mol.

Based on the above investigation, Path B-III is favorable for the $B(C_6F_5)_3$/C bonding

involved mechanism. It includes successive steps of N_2 elimination, $B(C_6F_5)_3$/C1 bonding, electrophilic attack and proton transfer. The overall energy changes is -52.3 kcal/mol (**1→3**). The rate-determining step is electrophilic attack with total energy barrier of 41.8 kcal/mol (**B-Int3→B-TS3**).

3.3 Mechanism of Path C ($B(C_6F_5)_3$/C=O bonding involved)

In Sections 3.1 and 3.2, the $B(C_6F_5)_3$/N bonding and $B(C_6F_5)_3$/C bonding involved mechanisms Path A and Path B were investigated respectively. The corresponding total energy barriers are 44.9 kcal/mol (**1→A-TS2**) and 42.7 kcal/mol (**B-Int3→B-TS3**) for Path A and Path B-III, respectively. The high energy barriers indicate that these mechanisms are unfavorable. Considering the $B(C_6F_5)_3$/C=O bonding is far away from the reaction center of electrophilic attack with smaller steric hindrance, we further investigated the $B(C_6F_5)_3$/C=O bonding initiated mechanism (Path C).

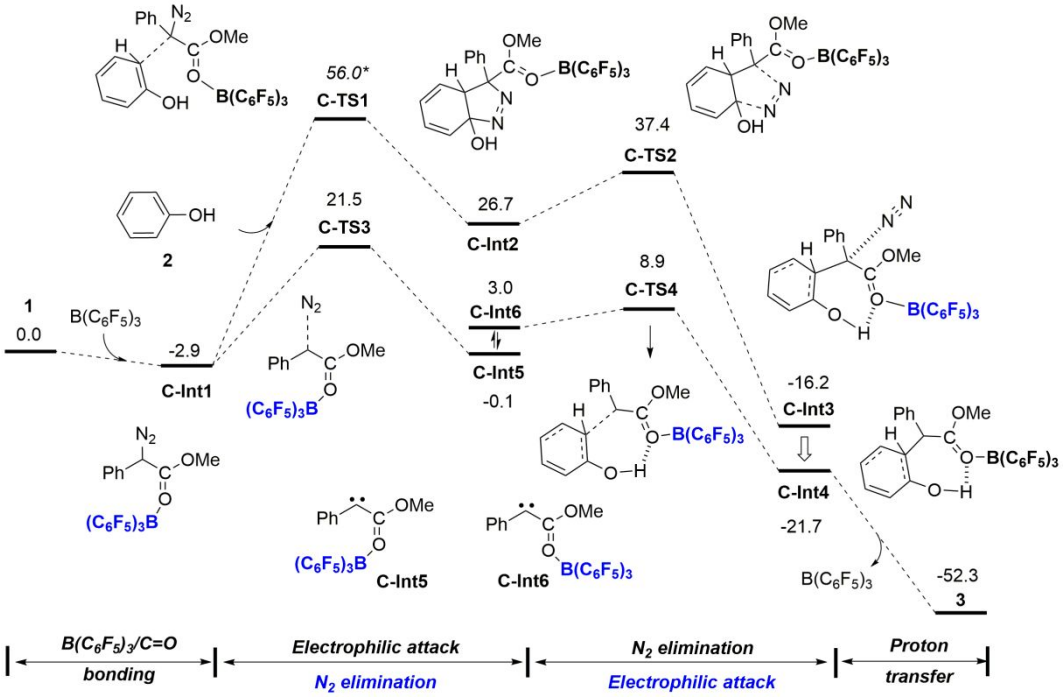

Figure 5 The energy profiles of $B(C_6F_5)_3$/C=O bonding involved mechanism (Path C, in kcal/mol)

As mentioned in the introduction, Path C shows the "$B(C_6F_5)_3$/C=O bonding-electrophilic attack-C−H cleavage" process. As shown in Figure 5, $B(C_6F_5)_3$ firstly coordinates with carbonyl group to give intermediate **C-Int1** with free energy of -2.9 kcal/mol. The stretched C1−N1 bond

(from 1.32 Å of **1** to 1.33 Å of **C-Int1**) indicates that $B(C_6F_5)_3$/C=O bonding reduces the steric hindrance around C1 atom by stretching the C1−N1 bond (Figure 6). From **C-Int1**, two mechanisms were investigated (Path C-I and C-II). In Path C-I, **C-Int1** first goes through electrophilic attack and N_2 elimination followed. While in Path C-II, electrophilic attack occurs after N_2 elimination.

For Path C-I, electrophilic attack occurs via transition state **C-TS1** in which C1 atom of diazoester attacks *ortho*-C2 atom of phenol substrate **2**. However, the transition state cannot be located. After optimization, the cyclic intermediate **C-Int2** is always obtained with free energy of 26.7 kcal/mol. In **C-Int2**, C1−C2 bond forms and terminal N2 atom bonds to benzene ring. To estimate the energy requirements of the electrophilic attack, we performed energy scan of the C1−C2 bonding process. It is found that the highest energy point is 56.0 kcal/mol with C1−C2 bond length of 2.00 Å (**C-TS1** in Figure 5).[33] At this point, the C1−N1 bond stretches to 1.36 Å from 1.33 Å of intermediate **C-Int1**. For the cyclic intermediate **C-Int2**, C1−N1 and C3−N2 bonds are formed with bond lengths of 1.53 Å and 1.52 Å, respectively (Figure 6). N_2 elimination then occurs on **C-Int2** via transition state **C-TS2** with free energy of 37.4 kcal/mol. In **C-TS2**, C1−N1 and C3−N2 bonds stretch to 1.88 Å and 1.74 Å, respectively. After N_2 elimination, intermediate **C-Int3** is obtained with highly decreased free energy of -16.2 kcal/mol. In intermediate **C-Int3**, the N_2 group is far from the C1 atom with C1⋯N≡N distance between of 3.92 Å. N_2 molecule then leaves to give intermediate **C-Int4** with decreased free energy of -21.7 kcal/mol. Finally, the $B(C_6F_5)_3$ group dissociation and proton transfer occur on **C-Int4** to yield product **3** with free energy of -52.3 kcal/mol. Accordingly, Path C-I includes the successive $B(C_6F_5)_3$/C=O bonding, electrophilic attack, N_2 elimination and proton transfer steps. The rate-determining step is electrophilic attack with total energy barrier of 58.9 kcal/mol (**C-Int1**→**C-TS1**).

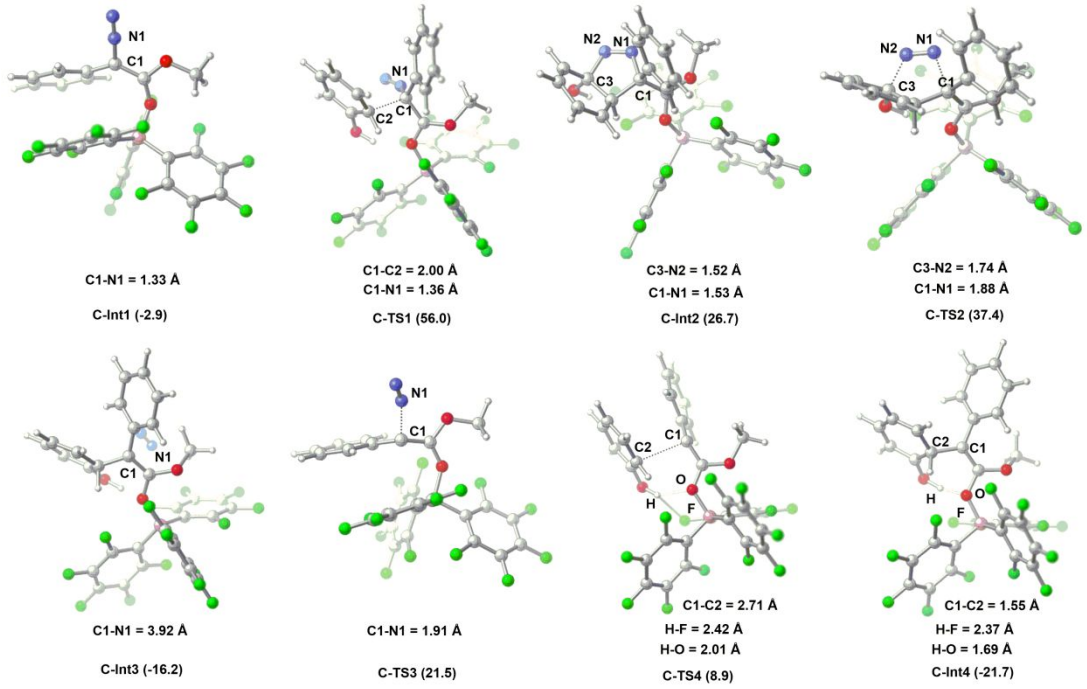

Figure 6 Optimized structures for selected species of Path C. Bond lengths are given in Å

Considering the weakening effect of $B(C_6F_5)_3$/C=O bonding on C1−N1 bond and the large energy barrier of direct electrophilic attack of **C-Int1**(in Path C-I), we then investigated Path C-II in which electrophilic attack occurs after N_2 elimination.

As shown in Figure 5, from **C-Int1**, N_2 elimination occurs via transition state **C-TS3**. The C1−N1 distance extends to 1.91 Å in **C-TS3** (Figure 6). The free energy of the transition state is 21.5 kcal/mol, and the energy barrier of this step is 24.4 kcal/mol (**C-Int1**→**C-TS3**). After N_2 elimination, intermediate **C-Int5** is obtained with free energy of -0.1 kcal/mol. **C-Int5** undergoes isomerization to give **C-Int6** for the following electrophilic attack. The free energy of **C-Int6** is 3.0 kcal/mol. Then, **C-Int6** goes through electrophilic attack via transition state **C-TS4** with C1−C2 distance of 2.71 Å. It is worth noting that O−H···O hydrogen bond exists between OH and carbonyl O atom with H···O distance of 2.01 Å. In addition, O−H···F hydrogen bond exists between OH and -C_6F_5 group with H···F distance of 2.42 Å (Figure 6). The free energy of **C-TS4** is 8.9 kcal/mol, and the energy barrier of this step is 11.8 kcal/mol (**C-Int1**→**C-TS4**). After the electrophilic attack, the C1−C2 bonded intermediate **C-Int4** is obtained with decreased free energy of -21.7 kcal/mol. The C1−C2 bond shortens to 1.55 Å in intermediate **C-Int4**. The O−H···O and O-H···F hydrogen bonds still exist with H···O distance of 1.69 Å and H···F distance of

2.37 Å, respectively (Figure 6). Finally, **C-Int4** undergoes $B(C_6F_5)_3$ dissociation and proton transfer to give product **3** with decreased free energy of -52.3 kcal/mol. Accordingly, Path C-II includes the successive $B(C_6F_5)_3$/C=O bonding, N_2 elimination, electrophilic attack and proton transfer steps. The N_2 elimination step is the rate-determining step, and the total energy barrier is 24.4 kcal/mol (**C-Int1→C-TS3**).

In summary, the total energy barriers of Path C-I and Path C-II are 58.9 kcal/mol (**C-Int1→C-TS1**) and 24.4 kcal/mol (**C-Int1→C-TS3**), respectively. Therefore, Path C-II is more favorable. The advance N_2 elimination generates carbene intermediate, contributing to the following electrophilic attack.

3.4 Discussions on the favorable mechanism

According to the investigation results of section 3.1-3.3, Path A undergoes $B(C_6F_5)_3$/N bonding, electrophilic attack, N_2 elimination and proton transfer steps. The N_2 elimination step is the rate-determining step, with energy barrier of 44.9 kcal/mol (**1→A-TS2**). For Path B, Path B-III process is more favorable (than Path B-I and II), in which N_2 elimination, $B(C_6F_5)_3$/C1 bonding, electrophilic attack and proton transfer steps occur successively. The Electrophilic attack is rate-determining step with energy barrier of 42.7 kcal/mol (**B-Int3→B-TS3**). For Path C, Path C-II is more favorable (than Path C-I). It undergoes the $B(C_6F_5)_3$/C=O bonding, N_2 elimination, electrophilic attack and proton transfer steps. The N_2 elimination is the rate-determining step, with energy barrier of 24.4 kcal/mol (**C-Int1→C-TS3**). In summary, the Path C-II has the lowest total energy barrier and it is the favorable mechanism.

According to the obtained favorable mechanism, some experimental observations in Zhang' reactions can be well understood. First, the reaction does not exhibit kinetic isotope effect. It is understandable because N_2 elimination step is the rate-determining step in which the C-H cleavage is not involved. Second, the competition experiments of phenol and anisole shows higher reactivity of phenol than anisole. The free energies of the corresponding electrophilic attack transition state **C-TS4 and C-TS4-Me** for phenol and anisole are 8.9 kcal/mol and 13.5 kcal/mol, respectively. The latter is 4.6 kcal/mol higher than the former (See Supporting Information for more details). Considering the electrophilic attack is an irreversible step, the phenol with lower

energy barrier preferentially participates in the reaction. Thus, it is understandable that the anisole has much lower reactivity than phenol. Third, the reaction between diazoester and anisole give major product of water insertion and minor product of anisole alkylation. Calculation of water insertion shows the free energy of corresponding electrophilic attack transition state **C-TS4-H_2O** is 9.8 kcal/mol. It is lower than that of anisole (13.5 kcal/mol), which is consistent with the experiment that water insertion was mainly obtained (See Supporting Information for more details). Finally, there is no -C_6F_5 migration product in experiment. The phenomenon is expected because the $B(C_6F_5)_3$/carbonyl bonding effectively avoids -C_6F_5 migration (whereas $B(C_6F_5)_3$/C bonding leads to -C_6F_5 migration).[34]

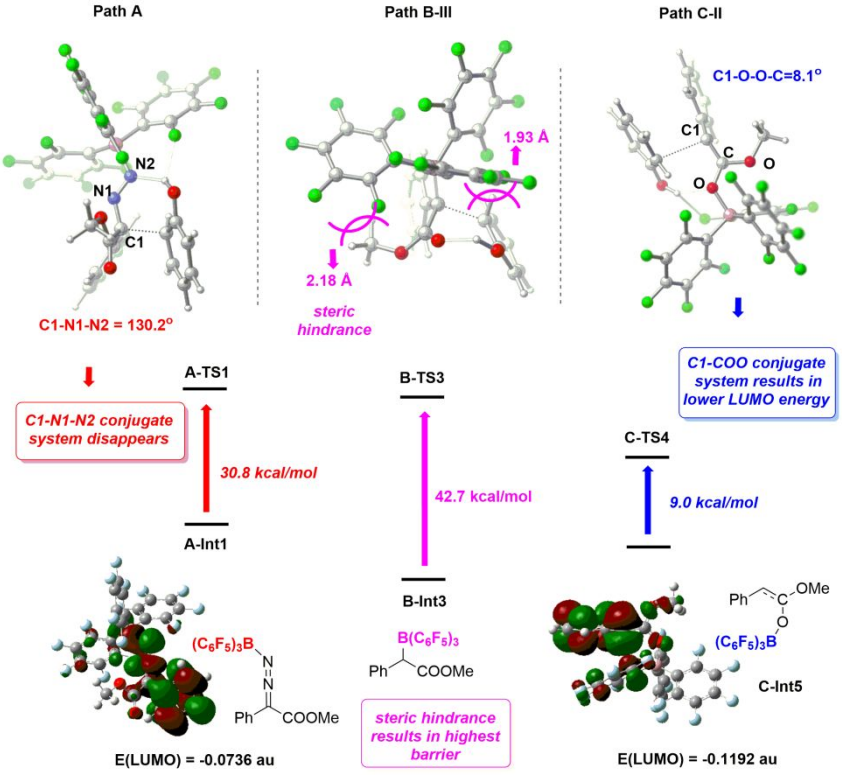

Figure 7 The comparison of electrophilic attack steps between Path A-C

Comparing Path A, B-III and Path C-II, we found that different coordination modes of $B(C_6F_5)_3$ with the diazoester directly affect the energy barrier of the electrophilic attack step. As shown in Figure 7, for $B(C_6F_5)_3$/N bonding in Path A, the elemental energy barrier of electrophilic attack step is 30.8 kcal/mol (**A-Int1**→**A-TS1**). For $B(C_6F_5)_3$/C bonding in Path B-III, the energy barrier is 42.7 kcal/mol (**B-Int3**→**B-TS3**). In contrast, for $B(C_6F_5)_3$/C=O bonding in Path C-II, the elemental energy barrier is only 9.0 kcal/mol (**C-Int5**→**C-TS4**). Investigation of corresponding

electrophilic attack transition states helps to reveal the origin of the favorable mechanism. For Path B-III with the highest energy barrier (in purple, Figure 7), $B(C_6F_5)_3$ directly bonds to C1 atom, resulting in large steric hindrance between $B(C_6F_5)_3$ and the phenol or diazoester in transition state **B-TS3**. The shortest distances between $B(C_6F_5)_3$ and these two substrate parts are 1.93 Å and 2.18 Å, respectively. For comparison, the distances are above 3.0 Å for **A-TS1** and **C-TS4** in Path A and Path C-II.

Comparison of **A-TS1** and **C-TS4** in Path A and Path C-II tells more information. For **A-TS1** of Path A (in red, Figure 7), the $B(C_6F_5)_3$/N bonding leads to the damage of the originally existing C1−N1−N2 conjugate system with decreased C1−N1−N2 angle of 130.2 in the transition state. However, for **C-TS4** of Path C-II (in blue, Figure 7), the $B(C_6F_5)_3$/C=O bonding causes the conjugated system formation between C1 and the COO group with small C1−O−O−C dihedral angle of 8.1°. On the other hand, for the pre-intermediate **A-Int1** and **C-Int5** of transition state **A-TS1** and **C-TS4**, the energies of the corresponding LUMO orbital are -0.0736 and -0.1192, respectively. The latter is significantly lower than the former, which is due to that the electron-withdrawing $B(C_6F_5)_3$ reduced the LUMO orbital energy through the conjugated system in **C-Int5**.[35] Considering the HOMO orbital energy of -0.21861 for the phenol substrate, the energy gap between phenol and intermediate **C-Int5** is lower, which also contributes to the lower energy barrier of Path C-II.

In summary, the $B(C_6F_5)_3$/C bonding results in large steric hindrance between $B(C_6F_5)_3$ and the substrates. $B(C_6F_5)_3$/N bonding damages the originally existing C1−N1−N2 conjugate system. In comparison, the $B(C_6F_5)_3$/C=O bonding reduces the steric hindrance during electrophilic attack. Additionally it causes the conjugated system formation between C1 and COO group, through which the LUMO orbital energy is reduced with the electron-withdrawing $B(C_6F_5)_3$ coordination. These two factors contributes to the favorable electrophilic attack with $B(C_6F_5)_3$/C=O bonding.

3.5 Discussions on regio-selectivity and chemo-selectivity

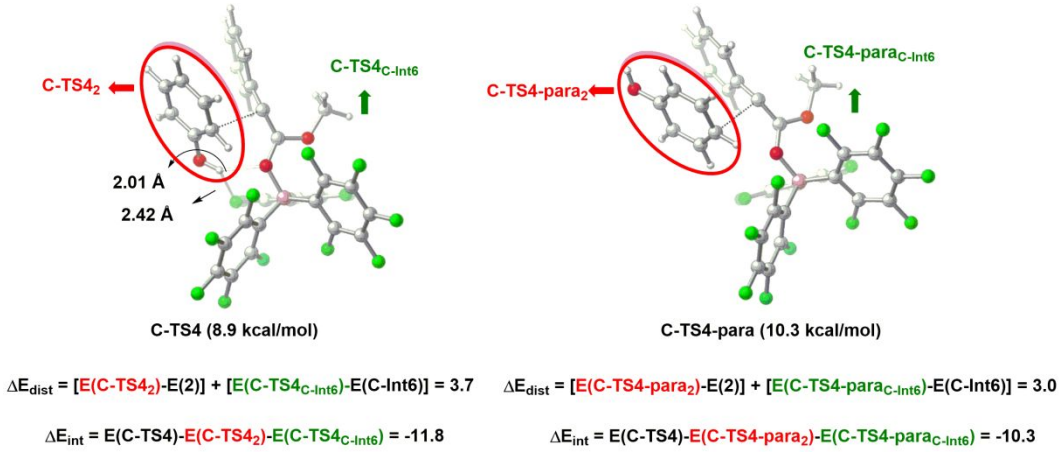

Figure 8 The Distortion/Interaction analysis of **C-TS4** and **C-TS4-para** (**C-TS4$_2$** and **C-TS4$_{C\text{-}Int6}$**, **C-TS4-para$_2$** and **C-TS4-para$_{C\text{-}Int6}$** are transition state fragments corresponding to **2** and **C-Int6**, the energies are given in kcal/mol).

According to the calculation results of 3.1-3.4, Path C-II is the favorable mechanism which includes the $B(C_6F_5)_3$/C=O bonding, N_2 elimination, electrophilic attack and proton transfer steps. The N_2 elimination step is rate-determining step. Meanwhile, the electrophilic attack step is selectivity-determining step. Herein, we focus on the electrophilic attack step to investigate the origins of regio-selectivity and chemo-selectivity.

For the regio-selectivity, as shown in Figure 8, the free energy of *ortho*-selective electrophilic attack transition state **C-TS4** is 8.9 kcal/mol. The *para*-selective electrophilic attack transition state is **C-TS4-para** with free energy of 10.3 kcal/mol. The latter is 1.4 kcal/mol higher than the former (10.3 vs 8.9 kcal/mol), which is consistent with the experiments that *ortho*-alkylation product is favorably yielded. To explore the origins for regio-selectivity, we performed Distortion/Interaction analysis [36] of **C-TS4** and **C-TS4-para**. The analysis quantifies two parts that contribute to the reaction energy barrier. On one hand, the energy consumption (Distortion energy, ΔE_{dist}) refers to the energy required to distort the substrates into corresponding fragments in the transition state. Here, ΔE_{dist} specifically refers to energy from **C-Int6** and **2** to **C-TS4$_{C\text{-}Int6}$** and **C-TS4$_2$** for *ortho*-selectivity, and to **C-TS4-para$_{C\text{-}Int6}$** and **C-TS4-para$_2$** for *para*-selectivity. On the other hand, the acquisition of energy (Interaction energy, ΔE_{int}) refers to the energy released by the transition state fragments forming a complete transition state. Here, ΔE_{int} is specifically the energy between **C-TS4$_{C\text{-}Int6}$+C-TS4$_2$** and **C-TS4** for *ortho*-selectivity, and **C-TS4-para$_{C\text{-}Int6}$+C-TS4-para$_2$** and **C-TS4-para** for *para*-selectivity. For **C-TS4** and

C-TS4-para, the ΔE_{dist} are 3.7 kcal/mol and 3.0 kcal/mol, the ΔE_{int} are -11.8 kcal/mol and -10.3 kcal/mol, respectively.[37] Therefore, even though the greater ΔE_{dist}(**C-TS4**) than ΔE_{dist}(**C-TS4-para**), the larger ΔE_{int}(**C-TS4**) than ΔE_{int}(**C-TS4-para**) leads to the lower energy barrier of **C-TS4**. Therefore, the interaction energy mainly contributes to the favorable *ortho*-selective electrophilic attack process.

The interaction effect difference between **C-TS4** and **C-TS4-para** reflects in two aspects: (1) the forming C-C bond interaction and (2) hydrogen bond interaction. For C-C interaction, we compare the NBO charge of the *ortho*-C and *para*-C of phenol substrate. The former is higher than the latter (-0.301 vs -0.261), which causes greater interaction between *ortho*-C and the electrophilic carbene C atom. It is consistent with the larger distortion energy of phenol in **C-TS4** (ΔE_{dist}(**C-TS4$_2$**) and ΔE_{dist}(**C-TS4-para$_2$**) are 0.9 and 0.4 kcal/mol, respectively). As to hydrogen bond interaction, for the *ortho*-selective **C-TS4**, O−H ⋯ O hydrogen bond interaction exists between OH and carbonyl O atom with H⋯O distance of 2.01 Å. The O−H⋯F hydrogen bond interaction exists between OH and F atom of $-C_6F_5$ group with H ⋯ F distance of 2.42 Å. In contrast, for the *para*-selective **C-TS4-para**, the interaction does not exist since the -OH group gets away from the ester group and $-C_6F_5$ group. To exclude the C-C interaction and examine the role of hydrogen bond alone, we compared the two pre-intermediates of transition states **C-TS4** and **C-TS4-para** (**C-TS4$_{pre}$** and **C-TS4-para$_{pre}$**, see Supporting Information for details). The O-H⋯O and O−H⋯F distances in **C-TS4$_{pre}$** are 2.14 and 2.67 Å, respectively. While, there is no hydrogen bond in **C-TS4-para$_{pre}$**. The energy of the latter is 1.5 kcal/mol higher than the former, indicating the stabilization effect of hydrogen bond interaction. In summary, the greater *ortho*-C-C interaction and the hydrogen bond interaction of O−H⋯O and O−H⋯F jointly contribute to the favorable *ortho*-selective electrophilic attack.

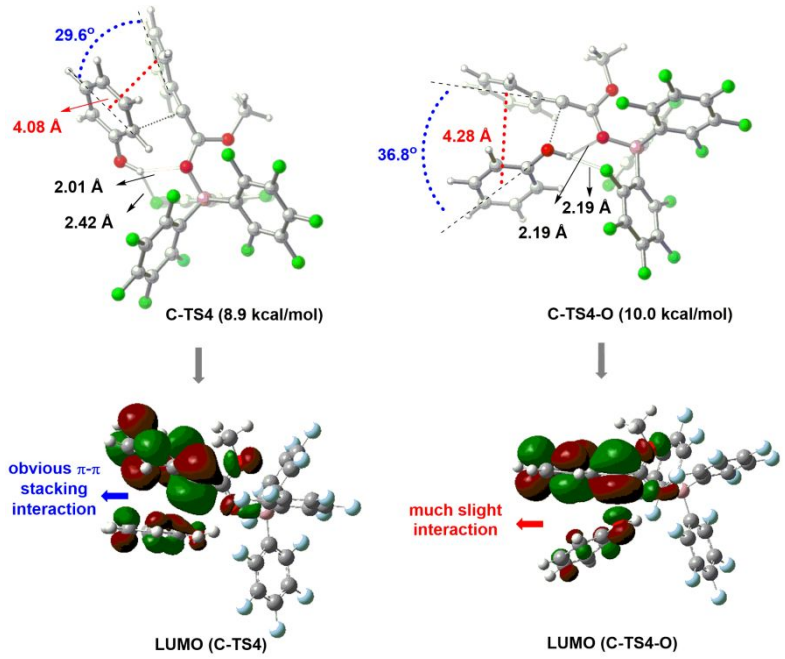

Figure 9 The structure and frontier orbital analysis of transition states **C-TS4** and **C-TS4-O**

For the chemo-selectivity, the electrophilic attack to the hydroxyl group of phenol substrate is investigated (Figure 9). The corresponding transition state is **C-TS4-O** with free energy of 10.0 kcal/mol. It is 1.1 kcal/mol higher than that of **C-TS4** (8.9 kcal/mol). The Distortion/Interaction analysis of **C-TS4** and **C-TS4-O** was also performed to explore the origins of chemo-selectivity.[38] The ΔE_{dist} of **C-TS4** is higher than that of **C-TS4-O** (3.7 vs 3.0 kcal/mol), and the ΔE_{int} of **C-TS4** is also higher (-11.8 vs -10.3 kcal/mol). Therefore, the larger interaction energy ΔE_{int} contributes to the lower energy barrier of the chemo-selective C-C electrophilic attack process. For the interaction difference between the two transition states, in addition to (1) the forming C-C/C-O bond interaction and (2) hydrogen bond interaction, (3) the π-π stacking between two benzene rings is also included. For the C-C/C-O interaction, since C and O are different elements and the chemical environment is different, the NBO charge is not compared here. In the phenol molecule, the oxygen atom with lone pair electrons forms a large π-bond with the benzene ring, which increases the charge density and nucleophilicity of the benzene ring. In **C-TS4**, the C-OH distance is shortened compared to phenol (1.366 vs 1.353 Å), whereas in **C-TS4-O**, the distance is longer than that of phenol (1.366 vs 1.369 Å). In other words, the conjugation between O and benzene ring is enhanced during C-C bonding while the C-O bonding weakens the original conjugation in phenol. It contributes to the stronger C-C interaction than the C-O interaction. This is consistent

with the lower energy of the post-intermediate after C-C bonding (the energy of the post-intermediates **C-Int4** and **C-Int4-O** after C-C/C-O bonding are -21.7 and -7.0 kcal/mol, respectively)[39]. For hydrogen bond interaction, in **C-TS4-O**, O−H···O and O−H···F distance are 2.19 (2.188) and 2.19 (2.189) Å, respectively. The distances are shorter than that of **C-TS4 (**2.01 and 2.42 Å), indicating that the stronger stabilization effect of hydrogen bonds in **C-TS4-O**. For the π-π stacking between two benzene rings of phenol and diazoester, the interaction is more obvious for **C-TS4** than **C-TS4-O**. As shown in Figure 9, for **C-TS4**, the distance between the centers of two benzene rings is 4.08 Å, the angle between the benzene ring planes is 29.6°. In **C-TS4-O**, the distance between the two benzene rings is larger (4.28 Å), and the angle between them is larger (36.8°). The frontier LUMO orbital of these two transition states shows that the π-π orbital interaction between the two benzene rings of **C-TS4** is more obvious than that of **C-TS4-O**. In summary, although the stronger hydrogen bond interaction in the C-O electrophilic attack transition state, the greater C-C interaction and the π-π stacking between the benzene rings concerted contribute to the favorable C-C electrophilic attack.

According to the above analysis and discussions, it is revealed that the *ortho*-selectivity is resulted from the greater *ortho*-C-C interaction (than *para*-C-C interaction) and the O−H···O and O−H···F hydrogen bonding during electrophilic attack process. The greater C-C interaction (than C-O interaction) and the π-π stacking between the benzene ring of phenol and diazoester concerted contribute to the chemo-selective C-C electrophilic attack.

4. Conclusion

The $B(C_6F_5)_3$-mediated *ortho*-selective C−H alkylation of unprotected phenols with diazoesters provides an important alternative route for the derivatization of phenols. To elucidate the detailed reaction mechanism and origin of chemo- and regio-selectivity, the theoretical calculations were carried out. It is found that the reaction undergoes $B(C_6F_5)_3$/C=O bonding involved mechanism, rather than the previously proposed $B(C_6F_5)_3$/N or $B(C_6F_5)_3$/C bonding involved mechanisms. The favorable mechanism includes the $B(C_6F_5)_3$/C=O bonding, N_2 elimination, electrophilic attack and proton transfer steps. Further mechanistic origin investigation reveals that the $B(C_6F_5)_3$/C=O bonding reduces the steric hindrance during electrophilic attack, and decreases the LUMO orbital energy via the electron-withdrawing effect of $B(C_6F_5)_3$ by

forming conjugated system. The *ortho*-selectivity is mainly resulted from greater *ortho*-C-C interaction (than *para*-C-C) and the hydrogen bond interaction of O−H ⋯ O and O−H ⋯ F. The chemo-selectivity is due to greater C-C interaction (than C-O interaction) and the π-π stacking between the benzene ring of phenol and diazoester.

Supporting Information

The Supporting Information is available free of charge on the ACS Publications website. The test calculations about the DFT approach, energy profiles for the reaction of anisole and water, The complete content of reference 37,38 and 39, 3D structures of **C-TS4$_{pre}$** and **C-TS4-para$_{pre}$**, and Cartesian coordinates, free energies, and thermal corrections.

Corresponding Author

*E-mail: jqliu@hfut.edu.cn.

*E-mail: qfnu_yuanyejiang@163.com.

Notes

These two authors Qi Zhang and Xiao-Fei Zhang contribute equally to this study. The authors declare no competing financial interests.

Acknowledgements

We thank the NSFC (21702041, 21702119), the Natural Science Foundation of Shandong Province (No. ZR2017QB001), 111 Project “New Materials and Technology for Clean Energy” (B18018), the Key Laboratory of Advanced Functional Materials and Devices of Anhui Province (No. PA2017AKZS0001). This work is also supported by the Fundamental Research Funds for the Central Universities of China (No. JZ2018HGBZ0100, No. PA2019GDPK0052). The numerical calculations in this paper have been done on the supercomputing system in the National Supercomputing Center in Shenzhen. We thank Prof. Junliang Zhang for the helpful discussions.

References

(1) (a) Godula, K.; Sames, D. C-H Bond Functionalization in Complex Organic Synthesis. *Science* **2006**, *312*, 67-72. (b) Davies, H. M. L.; Manning, J. R. Catalytic C-H Functionalization by Metal Carbenoid and Nitrenoid Insertion. *Nature* **2008**, *451*, 417-424. (c)

Leow, D.; Li, G.; Mei, T.-S.; Yu, J.-Q. Activation of Remote meta-C-H Bonds Assisted by an End-On Template. *Nature* **2012**, *486*, 518-522. (d) McNally, A.; Haffemayer, B.; Collins, B. S. L.; Gaunt, M. J. Palladium-Catalysed C-H Activation of Aliphatic Amines to Give Strained Nitrogen Heterocycles. *Nature* **2014**, *510*, 129-133. (e) Fu, J.; Ren, Z.; Bacsa, J.; Musaev, D. G.; Davies, H. M. L. Desymmetrization of Cyclohexanes by Site- and Stereoselective C-H Functionalization. *Nature* **2018**, *564*, 395-399.

(2) (a) Saint-Denis, T. G.; Zhu, R.-Y.; Chen, G.; Wu, Q.-F.; Yu, J.-Q. Enantioselective C(sp^3)-H Bond Activation by Chiral Transition Metal Catalysts. *Science* **2018**, *359*, eaao4798. (b) Hu, Y.; Zhou, B.; Wang, C. Inert C-H Bond Transformations Enabled by Organometallic Manganese Catalysis. *Acc. Chem. Res.* **2018** *513*, 816-827. (c) Gensch, T.; Hopkinson, M. N.; Glorius, F.; Wencel-Delord, J. Mild Metal-Catalyzed C-H Activation: Examples and Concepts. *Chem. Soc. Rev.* **2016**, *45*, 2900-2936.

(3) (a) Shan, C.; Zhu, L; Qu, L.-B.; Bai, R.; Lan, Y. Mechanistic View of Ru-Catalyzed C-H Bond Activation and Functionalization: Computational Advances. *Chem. Soc. Rev.* **2018**, *47*, 7552-7576. (b) Qi, X.; Li, Y.; Bai, R.; Lan, Y. Mechanism of Rhodium-Catalyzed C-H Functionalization: Advances in Theoretical Investigation. *Acc. Chem. Res.* **2017**, *50*, 2799-2808.

(4) Yamaguchi, J.; Yamaguchi, A. D.; Itami, K. C-H Bond Functionalization: Emerging Synthetic Tools for Natural Products and Pharmaceuticals. *Angew. Chem. Int. Ed.* **2012**, *51*, 8960-9009.

(5) (a) Abrams, D. J.; Provencher, P. A.; Sorensen, E. J. Recent Applications of C-H Functionalization in Complex Natural Product Synthesis. *Chem. Soc. Rev.* **2018**, *47*, 8925-8967. (b) Sinha, S. K.; Zanoni, G.; Maiti, D. Natural Product Synthesis by C-H Activation. *Asian J. Org. Chem.* **2018**, *7*, 1178-1192.

(6) Gandeepan, P.; Müller, T.; Zell, D.; Cera, G.; Warratz, S.; Ackermann, L. 3d Transition Metals for C-H Activation. *Chem. Rev.* **2019**, *119*, 2192-2452.

(7) Davies, D. L.; Macgregor, S. A.; McMullin, C. L. Computational Studies of Carboxylate-Assisted C-H Activation and Functionalization at Group 8-10 Transition Metal Centers. *Chem. Rev.* **2017**, *117*, 8649-8709.

(8) (a) Bose, S. K.; Marder, T. B. A Leap Ahead for Activating C-H Bonds. *Science* **2015**,

349, 473-474. (b) Stephan, D. W. The Broadening Reach of Frustrated Lewis Pair Chemistry. *Science* **2016**, *354*, aaf7229.

(9) (a) Qin, Y.; Zhu, L.; Luo, S. Organocatalysis in Inert C-H Bond Functionalization. *Chem. Rev.* **2017**, *117*, 9433-9520. (b) Légaré, M.-A.; Courtemanche, M.-A.; Rochette, É.; Fontaine, F.-G. Metal-Free Catalytic C-H Bond Activation and Borylation of Heteroarenes. *Science* **2015**, *349*, 513-516.

(10) (a) Dureen, M. A.; Stephan, D. W. Terminal Alkyne Activation by Frustrated and Classical Lewis Acid/Phosphine Pairs. *J. Am. Chem. Soc.* **2009**, *131*, 8396-8397. (b) Iashin, V.; Chernichenko, K.; Pápai, I.; Repo, T., Atom-Efficient Synthesis of Alkynylfluoroborates Using BF_3-Based Frustrated Lewis Pairs. *Angew. Chem. Int. Ed.* **2016**, *55*, 14146-14150. (c) Chan, J. Z.; Yao, W.; Hastings, B. T.; Lok, C. K.; Wasa, M. Direct Mannich-Type Reactions Promoted by Frustrated Lewis Acid/Brønsted Base Catalysts. *Angew. Chem. Int. Ed.* **2016**, *55*, 13877-13881.

(11) (a) Ménard, G.; Stephan, D. W. C-H Activation of Isobutylene Using Frustrated Lewis Pairs: Aluminum and Boron σ-Allyl Complexes. *Angew. Chem. Int. Ed.* **2012**, *51*, 4409-4412. (b) Rochette, É.; Courtemanche, M. A.; Fontaine, F. G. Frustrated Lewis Pair Mediated Csp^3-H Activation. *Chem. Eur. J.* **2017**, *23*, 3567-3571.

(12) (a) Campbell, I. B.; Macdonald, S. J. F.; Procopiou, P. A. Medicinal Chemistry in Drug Discovery in Big Pharma: Past, Present and Future. *Drug Discov. Today* **2018**, *23*, 219-234. (b) Caro-Diaz, E. J. E.; Urbano, M.; Buzard, D. J.; Jones, R. M. C-H Activation Reactions as Useful Tools for Medicinal Chemists. *Bioorg. Med. Chem. Lett.* **2016**, *26*, 5378-5383.

(13) (a) Légaré, M. A.; Courtemanche, M. A.; Rochette, É.; Fontaine, F. G. Metal-Free Catalytic C-H Bond Activation and Borylation of Heteroarenes. *Science* **2015**, *349*, 513-516. (b) Chernichenko, K.; Lindqvist, M.; Kótai, B.; Nieger, M.; Sorochkina, K.; Pápai, I.; Repo, T. Metal-Free sp^2-C-H Borylation as a Common Reactivity Pattern of Frustrated 2-Aminophenylboranes. *J. Am. Chem. Soc.* **2016**, *138*, 4860-4868. (c) Bähr, S.; Oestreich, M. Electrophilic Aromatic Substitution with Silicon Electrophiles: Catalytic Friedel-Crafts C-H Silylation. *Angew. Chem. Int. Ed.* **2017**, *56*, 52-59. (d) Ma, Y.; Wang, B.; Zhang, L.; Hou, Z., Boron-Catalyzed Aromatic C-H Bond Silylation with Hydrosilanes. *J. Am. Chem. Soc.* **2016**, *138*, 3663-3666.

(14) For reviews, see: a) Gillingham, D.; Fei, N. Catalytic X-H Insertion Reactions Based on Carbenoids. *Chem. Soc. Rev.* **2013**, *42*, 4918-4931. (b) Guo, X.; Hu, W. Novel Multicomponent Reactions via Trapping of Protic Onium Ylides with Electrophiles. *Acc. Chem. Res.* **2013**, *46*, 2427-2440. (c) Zhu, S.-F.; Zhou, Q.-L. Transition-Metal-Catalyzed Enantioselective Heteroatom-Hydrogen Bond Insertion Reactions. *Acc. Chem. Res.* **2012**, *45*, 1365-1377.

(15) (a) Davies, H. M. L.; Hansen, T.; Rutberg, J.; Bruzinski, P. R. Rhodium(II) (S)-N-(Arylsulfonyl)prolinate Catalyzed Asymmetric Insertion of Vinyl- and Phenylcarbenoids into the Si-H Bond. *Tetrahedron Lett.* **1997**, *38*, 1741-1744. (b) Ge, M.; Corey, E. J. A Method for the Catalytic Enantioselective Synthesis of 6-Silylated 2-Cyclohexenones. *Tetrahedron Lett.* **2006**, *47*, 2319-2321.

(16) (a) Zhu, S.-F.; Chen, W.-Q.; Zhang, Q.-Q.; Mao, H.-X.; Zhou, Q.-L. Enantioselective Copper Catalyzed O-H Insertion of R-Diazo Phosphonates. *Synlett* **2011**, *2011*, 919-922. (b) Chen, C.; Zhu, S.-F.; Liu, B.; Wang, L.-X.; Zhou, Q.-L. Highly Enantioselective Insertion of Carbenoids into O-H Bonds of Phenols: An Efficient Approach to Chiral α-Aryloxycarboxylic Esters. *J. Am. Chem. Soc.* **2007**, *129*, 12616-12617.

(17) Deng, Q.-H.; Xu, H.-W.; Yuen, A. W.-H.; Xu, Z.-J.; Che, C.-M. Ruthenium-Catalyzed One-Pot Carbenoid N-H Insertion Reactions and Diastereoselective Synthesis of Prolines. *Org. Lett.* **2008**, *10*, 1529-1532. (b) Austeri, M.; Rix, D.; Zeghida, W.; Lacour, J. CpRu-Catalyzed O-H Insertion and Condensation Reactions of α-Diazocarbonyl Compounds. *Org. Lett.* **2011**, *13*, 1394-1397.

(18) Zhu, S.-F.; Cai, Y.; Mao, H.-X.; Xie, J.-H.; Zhou, Q.-L. Enantioselective Iron-Catalysed O-H Bond Insertions. *Nat. Chem.* **2010**, *2*, 546-551.

(19) Schmidt, B.; Nave, S. Palladium-Catalyzed O-Allylation of R-Hydroxy Carbonyl Compounds. *Adv. Synth. Catal.* **2006**, *348*, 531-537.

(20) (a) Yu, Z.; Ma, B.; Chen, M.; Wu, H.-H.; Liu, L.; Zhang, J. Highly Site-Selective Direct C-H Bond Functionalization of Phenols with α-Aryl-α-diazoacetates and Diazooxindoles via Gold Catalysis. *J. Am. Chem. Soc.* **2014**, *136*, 6904-6907. (b) Liu, Y.; Yu, Z.; Zhang, J. Z.; Liu, L.; Xia, F.; Zhang, J. Origins of Unique Gold-Catalysed Chemo- and Site-Selective C-H Functionalization of Phenols with Diazo Compounds. *Chem. Sci.* **2016**, *7*, 1988-1995.

(21) Xi, Y.; Su, Y.; Yu, Z.; Dong, B.; McClain, E. J.; Lan, Y.; Shi, X. Chemoselective Carbophilic Addition of α-Diazoesters through Ligand-Controlled Gold Catalysis. *Angew. Chem. Int. Ed.* **2014**, *53*, 9817-9821.

(22) Yu, Z.; Li, Y.; Shi, J.; Ma, B.; Liu, L.; Zhang, J. $(C_6F_5)_3B$ Catalyzed Chemoselective and *ortho*-Selective Substitution of Phenols with α-Aryl α-Diazoesters. *Angew. Chem. Int. Ed.* **2016**, *55*, 14807-14811.

(23) Frisch, M. J.; Trucks, G. W.; Schlegel, H. B.; Scuseria, G. E.; Robb, M. A.; Cheeseman, J. R.; Scalmani, G.; Barone, V.; Mennucci, B.; Petersson, G. A.; Nakatsuji, H.; Caricato, M.; Li, X.; Hratchian, H. P.; Izmaylov, A. F.; Bloino, J.; Zheng, G.; Sonnenberg, J. L.; Hada, M.; Ehara, M.; Toyota, K.; Fukuda, R.; Hasegawa, J.; Ishida, M.; Nakajima, T.; Honda, Y.; Kitao, O.; Nakai, H.; Vreven, T.; Montgomery, J. A., Jr.; Peralta, J. E.; Ogliaro, F.; Bearpark, M.; Heyd, J. J.; Brothers, E.; Kudin, K. N.; Staroverov, V. N.; Keith, T.; Kobayashi, R.; Normand, J.; Raghavachari, K.; Rendell, A.; Burant, J. C.; Iyengar, S. S.; Tomasi, J.; Cossi, M.; Rega, N.; Millam, J. M.; Klene, M.; Knox, J. E.; Cross, J. B.; Bakken, V.; Adamo, C.; Jaramillo, J.; Gomperts, R.; Stratmann, R. E.; Yazyev, O.; Austin, A. J.; Cammi, R.; Pomelli, C.; Ochterski, J. W.; Martin, R. L.; Morokuma, K.; Zakrzewski, V. G.; Voth, G. A.; Salvador, P.; Dannenberg, J. J.; Dapprich, S.; Daniels, A. D.; Farkas, O.; Foresman, J. B.; Ortiz, J. V.; Cioslowski, J.; Fox, D. J. Gaussian 09, revision D.01. *Gaussian, Inc.: Wallingford CT* **2013**.

(24) (a) Becke, A. D. Becke's Three Parameter Hybrid Method Using the LYP Correlation Functional. *J. Chem. Phys.* **1993**, *98*, 5648-5652. (b) Lee, C.; Yang, W.; Parr, R. G. Results Obtained with the Correlation Energy Density Functionals. *Phys. Rev. B: Condens. Matter Mater. Phys.* **1988**, *37*, 785.

(25) B3LYP have been frequently used in previous theoretical study of Lewis acid catalysis and other metal free system, for examples, see: (a) Shen, L.; Zhao, K.; Doitomi, K.; Ganguly, R.; Li, Y.-X.; Shen, Z.-L.; Hirao, H.; Loh, T.-P. Lewis Acid-Catalyzed Selective [2+2]-Cycloaddition and Dearomatizing Cascade Reaction of Aryl Alkynes with Acrylates. *J. Am. Chem. Soc.* **2017**, *139*, 13570-13578. (b) Ahmed, J.; Chakraborty, S.; Jose, A.; P, S.; Mandal, S. K. Integrating Organic Lewis Acid and Redox Catalysis: The Phenalenyl Cation in Dual Role. *J. Am. Chem. Soc.* **2018**, *140*, 8330-8339. (c) Pogoreltsev, A.; Tulchinsky, Y.; Fridman, N.; Gandelman, M. Nitrogen Lewis Acids. *J. Am. Chem. Soc.* **2017**, *139*, 4062-4067. (d) Jiang,

Y.-Y.; Li, G.; Yang, D.; Zhang, Z.; Zhu, L.; Xia, F.; Bi, S., Mechanism of Cu-Catalyzed Aerobic C(CO)-CH_3 Bond Cleavage: A Combined Computational and Experimental Study. *ACS Catal.* **2019**, *9*, 1066-1080. (e) Zhang, Q.; Fu, M.-C.; Yu, H.-Z.; Fu, Y.; Mechanism of Boron-Catalyzed N-Alkylation of Amines with Carboxylic Acids. *J. Org. Chem.* **2016**, *81*, 6235-6243. (f) Zhang, Q.; Yu, H.-Z.; Fu, Y. NHC-Catalyzed Homoenolate Reaction of Enals and Nitroalkenes: Computational Study of Mechanism, Chemoselectivity and Stereoselectivity. *Org. Chem. Front.* **2014**, *1*, 614-624.

(26) Höllwarth, A.; Böhme, M.; Dapprich, S.; Ehlers, A. W.; Gobbi, A.; Jonas, V.; Kohler, K. F.; Stegmann, R.; Veldkamp, A.; Frenking, G. A Set of d-Polarization Functions for Pseudo-Potential Basis Sets of the Main Group Elements Al-Bi and f-Type Polarization Functions for Zn, Cd, Hg. *Chem. Phys. Lett.* **1993**, *208*, 237-240.

(27) Gonzalez, C.; Schlegel, H. B. Reaction Path Following in Mass-Weighted Internal Coordinates. *J. Phys. Chem.* **1990**, *94*, 5523-5527.

(28) (a) Zhao, Y.; Truhlar, D. G. The M06 Suite of Density Functionals for Main Group Thermochemistry, Thermochemical Kinetics, Noncovalent Interactions, Excited States, and Transition Elements: Two New Functionals and Systematic Testing of Four M06-Class Functionals and 12 other Functionals. *Theor. Chem. Acc.* **2008**, *120*, 215-241. (b) Zhao, Y.; Truhlar, D. G. Density Functionals with Broad Applicability in Chemistry. *Acc. Chem. Res.* **2008**, *41*, 157-167.

(29) The B3LYP//M06-2X method has been justified via test calculations (See Supporting Information for the details). Additionally, it has been frequently used in theoretical studies of organic reaction systems: (a) Um, J. M.; DiRocco, D. A.; Noey, E. L.; Rovis, T.; Houk, K. N. Quantum Mechanical Investigation of the Effect of Catalyst Fluorination in the Intermolecular Asymmetric Stetter Reaction. *J. Am. Chem. Soc.* **2011**, *133*, 11249-11254. (b) Krenske, E. H.; Houk, K. N.; Harmata, M. Computational Analysis of the Stereochemical Outcome in the Imidazolidinone-Catalyzed Enantioselective (4+3)-Cycloaddition Reaction. *J. Org. Chem.* **2015**, *80*, 744-750. (c) Xue, X.-S.; Yang, C.; Li, X.; Cheng, J.-P. Computational Study on the pK_a Shifts in Proline Induced by Hydrogen-Bond-Donating Cocatalysts. *J. Org. Chem.* **2014**, *79*, 1166-1173. (d) McIntosh, G. J.; Russell, D. K. Molecular Mechanisms in the Pyrolysis of Unsaturated Chlorinated Hydrocarbons: Formation of Benzene Rings. 1.

Quantum Chemical Studies. *J. Phys. Chem. A* **2013**, *117*, 4183-4197. (e) Lo, R.; Ganguly, B. In Silico Studies in Exploiting Weak Noncovalent C-H+···π and π-π Interactions To Achieve Dual Properties: Hyperbasicity and Multiple Dihydrogen Storage Materials with Paracyclophane-Based Carbene Derivatives. *J. Phys. Chem. C* **2013**, *117*, 19325-19333. (f) Flynn, B. L.; Manchala, N.; Krenske, E. H. Opposing Auxiliary Conformations Produce the Same Torquoselectivity in an Oxazolidinone-Directed Nazarov Cyclization. *J. Am. Chem. Soc.* **2013**, *135*, 9156-9163.

(30) The Mulliken charge has been frequently used in mechanistic analysis. (a) Watanabe, T.; Koyasu, K.; Tsukuda, T. Density Functional Theory Study on Stabilization of the Al13 Superatom by Poly(vinylpyrrolidone). *J. Phys. Chem. C* **2015**, *119*, 10904-10909. (b) Jiang, L.; Orimoto, Y.; Aoki, Y.; Substituent Effects on Menshutkin-Type Reactions in the Gas Phase and Solutions: Theoretical Approach from the Orbital Interaction View. *J. Chem. Theory Comput.* **2013**, *9*, 4035-4045. (c) Huang, H.-W.; Hsieh, H.-J.; Lin, I-H.; Tong, Y.-J.; Chen, H.-T. Hydrogen Adsorption and Storage in Heteroatoms (B, N) Modified Carbon-Based Materials Decorated with Alkali Metals: A Computational Study. *J. Phys. Chem. C* **2015**, *119*, 7662-7669. (d) Lee, B.; Yun, D.; Lee, J.-S.; Park, C. H.; Kim, T.-H. Development of Highly Alkaline Stable OH^--Conductors Based on Imidazolium Cations With Various Substituents for Anion Exchange Membranebased Alkaline Fuel Cells. *J. Phys. Chem. C* **2019**, *123*, 13508-13518.

(31) (a) Contreras-García, J.; Yang, W.; Johnson, E. R. Analysis of Hydrogen-Bond Interaction Potentials from the Electron Density: Integration of Noncovalent Interaction Regions. *J. Phys. Chem. A* **2011**, *115*, 12983-12990. (b) Wang, H.; Liu, S.; Zhao, Y.; Wang, J.; Yu, Z. Insights into the Hydrogen Bond Interactions in Deep Eutectic Solvents Composed of Choline Chloride and Polyols. *ACS Sustain. Chem. Eng.* **2019**, *7*, 7760-7767.

(32) Note that the scan is flexible scanning. The restrictive optimization of every point was done along the change of the specific geometric parameter (C1-B bond length herein). See supporting information for the energy scan process of the C1-B bonding process.

(33) See supporting information for the energy scan process of the the C1-C2 bonding process.

(34) (a) Elkin, P. K.; Levin, V. V.; Dilman, A. D.; Struchkova, M. I.; Elyakov, P. A.;

Arkhipov, D. E.; Korlyukov, A. A.; Tartakovsky, V. A. Reactions of CF_3-substituted boranes with α-diazocarbonyl compounds. *Tetrahedron Lett.* **2011**, *52*, 5259-5263. (b) Neu, R. C.; Jiang, C.; Stephan, D. W. Bulky Derivatives of Boranes, Boronic Acids and Boronate Esters via Reaction with Diazomethanes. *Dalton Trans.* **2013**, *42*, 726-736. (c) Peng, C.; Zhang, W.; Yan, G.; Wang, J. Arylation and Vinylation of α-Diazocarbonyl Compounds with Boroxines. *Org. Lett.* **2009**, *11*, 1667-1670.

(35) (a) Fujimoto, H. Frontier Orbitals and Reaction Paths: Selected Papers of Kenichi Fukui. *World Scientific Publishing Company Incorporated* **1997**. (b) Fukui, K. Role of Frontier Orbitals in Chemical Reactions. *Science* **1982**, *218*, 747-754.

(36) (a) Ess, D. N.; Houk, K. N. Distortion/Interaction Energy Control of 1,3-Dipolar Cycloaddition Reactivity. *J. Am. Chem. Soc.* **2007**, *129*, 10646-10647. (b) Gorelsky, S. I.; Lapointe, D.; Fagnou, K. Analysis of the Concerted Metalation-Deprotonation Mechanism in Palladium-Catalyzed Direct Arylation Across a Broad Range of Aromatic Substrates. *J. Am. Chem. Soc.* **2008**, *130*, 10848-10849. (c) Gorelsky, S. I.; Lapointe, D.; Fagnou, K. Analysis of the Palladium-Catalyzed (Aromatic)C–H Bond Metalation–Deprotonation Mechanism Spanning the Entire Spectrum of Arenes. *J. Org. Chem.* **2012**, *77*, 658-668.

(37) The detail fragmentation of **C-TS4** and **C-TS4-para** for the Distortion/Interaction analysis is shown in the supporting information.

(38) The detail fragmentation of **C-TS4-O** for the Distortion/Interaction analysis is shown in the supporting information.

(39) See supporting information for 3D structure of **C-Int4-O**.